Publication Year	2016
Acceptance in OA@INAF	2020-05-13T10:42:45Z
Title	The INTEGRAL/IBIS AGN catalogue: an update
Authors	MALIZIA, ANGELA; Landi, R.; Molina, M.; BASSANI, LOREDANA; BAZZANO, ANGELA; et al.
DOI	10.1093/mnras/stw972
Handle	http://hdl.handle.net/20.500.12386/24787
Journal	MONTHLY NOTICES OF THE ROYAL ASTRONOMICAL SOCIETY
Number	460

Monthly Notices of the ROYAL ASTRONOMICAL SOCIETY

MNRAS **460,** 19–29 (2016)
Advance Access publication 2016 April 23

doi:10.1093/mnras/stw972

The INTEGRAL/IBIS AGN catalogue: an update

A. Malizia,[1★] R. Landi,[1] M. Molina,[1★] L. Bassani,[1] A. Bazzano,[2] A. J. Bird[3] and P. Ubertini[2]

[1]*INAF/IASF-Bologna, Via P. Gobetti 101, I-40129 Bologna, Italy*
[2]*INAF/IASF-Roma, Via Fosso del Cavaliere 100, I-00133 Roma, Italy*
[3]*School of Physics and Astronomy, University of Southampton, SO17 1BJ Southampton, UK*

Accepted 2016 April 21. Received 2016 April 19; in original form 2016 February 2

ABSTRACT

In the most recent *IBIS* survey based on observations performed during the first 1000 orbits of *INTEGRAL*, are listed 363 high-energy emitters firmly associated with AGN, 107 of which are reported here for the first time. We have used X-ray data to image the *IBIS* 90 per cent error circle of all the AGN in the sample of 107, in order to obtain the correct X-ray counterparts, locate them with arcsec accuracy and therefore pinpoint the correct optical counterparts. This procedure has led to the optical and spectral characterization of the entire sample. This new set consists of 34 broad line or type 1 AGN, 47 narrow line or type 2 AGN, 18 blazars and 8 sources of unknown class. These eight sources have been associated with AGN from their positional coincidence with 2MASX/Radio/X-ray sources. Seven high-energy emitters have been included since they are considered to be good AGN candidates. Spectral analysis has been already performed on 55 objects and the results from the most recent and/or best statistical measurements have been collected. For the remaining 52 sources, we report the spectral analysis for the first time in this work. We have been able to obtain the full X-ray coverage of the sample making use of data from *Swift/XRT*, *XMM–Newton* and *NuSTAR*. In addition to the spectral characterization of the entire sample, this analysis has enabled us to identify peculiar sources and by comparing different data sets, highlight flux variability in the 2–10 keV and 20–40 keV bands.

Key words: catalogues – surveys – galaxies: active.

1 INTRODUCTION

In the last decade both *INTEGRAL/IBIS* (Ubertini et al. 2003) and *Swift/BAT* (Barthelmy et al. 2005), having good sensitivity and a wide-field sky coverage, were able to make progress in the high-energy domain (20–200 keV). In particular they have provided a great improvement in the knowledge of the high-energy extragalactic sky by detecting almost 1000 (mostly local) AGN at energies above 15 keV (Malizia et al. 2012; Baumgartner et al. 2013; this work).

Recently a new all sky *INTEGRAL* catalogue has been published (Bird et al. 2016) containing 939 hard X-ray selected sources of which 363 are definitely associated with AGN. Of these 107 have been reported for the first time as *INTEGRAL/IBIS* detections and another 7 objects are considered to be good candidate active galaxies. Thus extragalactic objects represent a significant fraction of the entire catalogue (about 40 per cent) and provide a well-defined sample of sources which can be used for statistical and population studies of AGN in many astrophysical contexts. In particular, the hard X-ray band is ideal to obtain information on the intrinsic column density of active galaxies (and hence its relation with other source parameters) since this waveband is the least affected by absorption. By comparing the hard X-ray emission with that of other wavebands, the *INTEGRAL* sample can be used for extensive correlation studies; it is also ideal for spectral analysis since this band is unique for studying spectral features such as the Compton reflection bump and the high-energy cut-off.

Fig. 1 shows the distribution of all AGN so far detected by *INTEGRAL* plotted on the sky; the stars represent the 107 new galaxies reported in this work, while the circles represent the AGN detected in the previous *IBIS* catalogues. The horizontal strip between $\pm 10^{\circ}$ in Galactic latitude is shown to highlight the so called Zone of Avoidance in the Galactic Plane where *INTEGRAL* plays a key role in detecting new absorbed objects and in particular AGN. In fact, due to observational strategy, *INTEGRAL* is more effective in finding hard X-ray emitting sources along the Galactic Plane and along the directions of the spiral arms while *Swift/BAT* is more effective at higher Galactic latitudes. Indeed among the 72 AGN detected by *INTEGRAL/IBIS* and not by *Swift/BAT*, almost 50 per cent

★ E-mail: malizia@iasfbo.inaf.it (AM); molina@iasfbo.inaf.it (MM)

© 2016 The Authors
Published by Oxford University Press on behalf of the Royal Astronomical Society

Downloaded from https://academic.oup.com/mnras/article-abstract/460/1/19/2608998 by guest on 29 April 2020

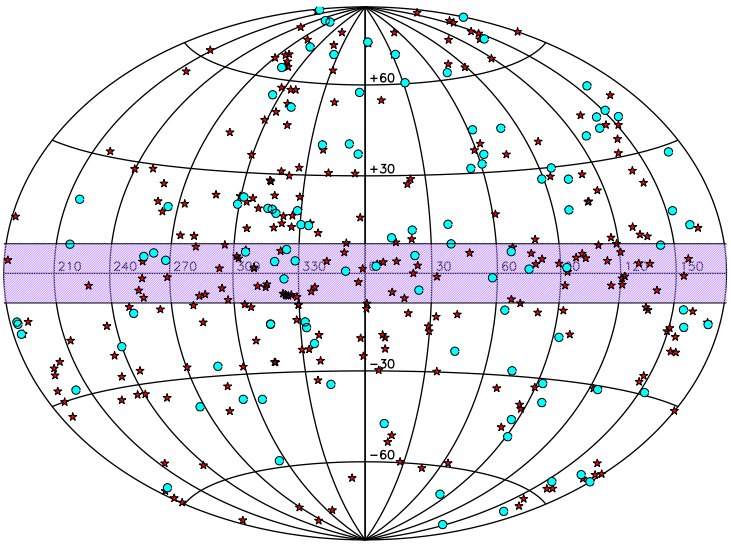

Figure 1. All the AGN so far detected by *INTEGRAL/IBIS* plotted on the sky. The stars represent the 107 new active galaxies studied in this work and first reported as *INTEGRAL* AGN in the last *IBIS* survey (Bird et al. 2016), while the circles are the AGN detected in previous surveys by *INTEGRAL/IBIS*.

(37 objects) are in the Galactic plane while the remaining sources are either detected as variable in the *IBIS* survey or are located in regions of the sky where *BAT* has less exposure.

A large fraction of the *INTEGRAL* AGN present in the new survey of Bird et al. (2016) have already been fully characterized in terms of optical and X-ray properties in Malizia et al. (2012), while the 107 new entries are presented and characterized in terms of their optical and X-ray properties in this paper where a few interesting objects are also highlighted and discussed.

2 *INTEGRAL* AGN UPDATE

In this paper we present the X-ray and optical follow-up work on 107 new AGN recently detected by *INTEGRAL*. Luckily, we have been able to obtain full X-ray coverage of the entire sample making use of data from *Swift/XRT*, *Newton–XMM* and *NuSTAR* archives or through *Swift/XRT* follow up observations triggered by us.

2–10 keV data are important for two main reasons: (1) they provide a unique tool to associate the high-energy source with a single/multiple X-ray counterpart, getting a better position and (2) to characterize the high-energy source at low energies, for example by estimating the spectral shape, the intrinsic absorption and the 2–10 keV flux/luminosity.

Association is a fundamental step in the analysis as it allows us to pinpoint the correct optical counterpart, locate it with arcsec accuracy and therefore provide a way to classify the source through optical spectroscopy. We have used the X-ray data to image the *IBIS* 90 per cent error circle of all AGN in the sample of 107 in order to determine the correct X-ray counterpart and in the majority of cases we found a single clear association. However, there were several sources where the *XRT* field of view contained more than one X-ray detection, thus deserving a deeper investigation. In these cases in order to pinpoint all counterparts and select the most likely, we superimposed the 99 per cent high-energy error circle on the 3–10 keV X-ray image. This allowed us to associate the hardest and the brightest X-ray source with the high-energy emitter. Generally secondary X-ray detections disappear above 3 keV or result in having a much lower signal to noise ratio with respect to the brightest source. This was the case for SWIFT J0444.1+2813, SWIFT J1630.5+3925, IGR J18078+1123, IGR J18308+0928 and SWIFT J1933.9+3258 where at energies higher than 3 keV a secondary X-ray object is still detected but only at lower significance level. We also note that in all but one case the X-ray counterpart was located well inside the *INTEGRAL* positional uncertainty; the only exception is SWIFT J1436.8-1615 for which a single X-ray source, a QSO at redshift of 0.144 54, was found just at the border of the *IBIS* error circle.

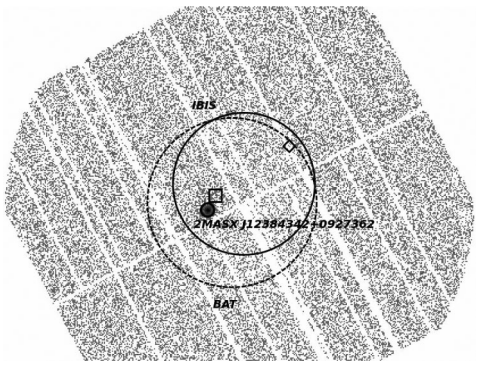

Figure 2. *XMM-pn* 4.5-10 keV image of the field around SWIFT J1238.6+0828. The solid and the dashed circles are the *IBIS* and *BAT* error circles, respectively. It is clear that there is only one X-ray detection corresponding to the Sey 2 galaxy 2MASX J12384342+0927362 at $z = 0.0829$. The box point shows the position of the galaxy cluster WHL J123841.5+092832 who does not emit any more at 4.5 keV, while the diamond point corresponds to the position of the galaxy VCC 1759, previously associated with SWIFT J1238.6+0828.

As a final remark, we note that this accurate method of association, led us to discover also an incorrect identification previously reported in the literature. This is the case of SWIFT J1238.6+0828 which has been associated with the galaxy VCC 1759 at $z = 0.0321$ (Baumgartner et al. 2013). From the inspection of the *XMM-pn* image there is no X-ray detection from VCC 1759 while there is 2–10 keV emission from the galaxy cluster WHL J123841.5+092832 at $z = 0.229\,900$ and from the Sey 2 galaxy 2MASX J12384342+0927362 at $z = 0.0829$. Both objects are well inside the *IBIS* and *BAT* error circles. As clearly shown in Fig. 2, which displays the *XMM-pn* 4.5-12 keV image, the most likely

Downloaded from https://academic.oup.com/mnras/article-abstract/460/1/19/2608998 by guest on 29 April 2020

X-ray counterpart of SWIFT J1238.6+0928 is the Sey 2 galaxy 2MASX J12384342+0927362, since the cluster is no longer detected above 4.5 keV.

Prior to characterizing each source spectrum at low energies, we have also pinpointed the correct optical counterpart and searched the literature and relevant archives for its appropriate classification. This has led to the optical characterization of almost all of the 107 new AGN. Optical classes have been mainly collected from NED (NASA Extragalactic data base), SIMBAD and from the 13th edition of the extragalactic catalogue of Véron-Cetty & Véron (2010). Table A1 lists all the new 107 AGN[1] together with their alternative names, coordinates,[2] redshift, class (columns from 2 to 6) and X-ray spectral parameters (columns 7–11, see Section 3). The *INTEGRAL/IBIS* 20-100 keV fluxes extracted from Bird et al. (2016) are reported in column 12, while in the last column (13) the references for the X-ray spectral parameters are listed. 88 AGN/candidate AGN were detected for the first time in the hard X-ray band by *INTEGRAL* and reported in Bird et al. (2016), while the remaining 26 objects, labelled in the Table A1 with the footnote [f], were already present in previous *IBIS* catalogues but only recently identified as active galactic nuclei and hence reported here as new *INTEGRAL* AGN. For 11 objects we have been able to secure optical follow up work and hence in these cases the source class is reported here for the first time while details of the optical spectra will be provided in a forthcoming paper by Masetti et al. (in preparation); these 11 objects have been labelled in the table with the footnote[e].

In Table A1 there are eight objects for which the optical class is still missing but their association with an AGN has been argued from different indicators such as the positional coincidence with a galaxy associated with a 2MASX extended object and/or with a radio source from which X-ray emission has been detected. Their class in Table A1 has been labelled as *AGN*. All but two of these sources where already known and extensively discussed in the literature (see their corresponding references). The two exceptions are IGR J17111+3910 and PBC J1850.7-1658: the first is positionally coincident with a *ROSAT* (1RXS J171105.6+390850) and a 2MASX source (2MASXJ17110531+3908488), while the second is associated with a bright radio source (NVSS J185054-165543) of 390 mJy flux at 20 cm. Both of them have an X-ray counterpart which has been observed by *Swift/XRT* and whose data have been analysed and presented in this work for the first time. For these eight AGN and four objects classified as blazars, redshift measurements are still missing.

Following our previous works (Malizia et al. 2007, 2012), this new set of AGN can be divided in 34 broad line or type 1 AGN (Seyfert 1-1.5), 47 narrow line or type 2 (type 1.8-2), 18 blazars and 8 sources of unknown class. KAZ 320 is the only Narrow Line Seyfert galaxy (NLS1) and is included in the type 1 AGN subset while the only Liner (NGC 5100), being absorbed, has been considered as a type 2 object.

2.1 AGN candidates

For the sake of completeness we have also added at the end of Table A1, seven sources which we consider to be good AGN candidates.

IGR J02447+7046 has been optically identified as a Sey 1.2 galaxy by Masetti et al. (2013) and indeed, analysing the *XRT* data, a soft X-ray source coincident with the optical position of this AGN has been marginally detected ($\sigma \sim 4$) although just outside the 90 per cent high-energy error circle. In order to improve the detection statistics, we have requested and obtained an extra *XRT* observation. The addition of these data reveals the presence of another X-ray source well inside the *IBIS* error box at a significance level of $\sim 4.4\sigma$ and positionally coincident with the radio source NVSS J024443+704946 having a 20-cm flux of 204 mJy. Since both sources weakly emit above 3 keV, are compatible with the *IBIS* error box and detected at almost the same significance level, we assume that both contribute to the high-energy emission. However, since IGR J02447+7046 is detected in a 3.4 d outburst in the IBIS survey (Bird et al. 2016) it is more likely that the high-energy emission is associated with a blazar type source that could possibly be linked to NVSS J025553+704946.

1RXS J112955.1-655542 has been considered as a candidate active galaxy since it is included in the WISE/2MASS/RASS AGN sample catalogue collected by Edelson & Malkan (2012) but it is the only object for which no X-ray information is available.

The remaining five objects have been proposed as AGN candidates in the literature before and the relevant reference for each one is reported in column 12 of Table A1.

3 X-RAY DATA ANALYSIS

For all the sample sources presented in this paper, we have collected the spectral properties in the contiguous 2–10 keV X-ray band in order to better characterize their nature and to search for spectral peculiarities. While for 55 objects, X-ray spectral analysis has already been performed and the results published, for the remaining 52 sources (almost half of the sample) we here report the X-ray spectral analysis for the first time. For the 55 already studied objects, spectral parameters are taken from the most recent and/or best statistical significance measurement (the relevant reference is reported in Table A1 as well as the instrument used). For all the remaining sources X-ray data have been retrieved from *Swift/XRT*, *Newton–XMM* and *NuSTAR* public archives available before the end of 2015. In cases where for a source we found observational data in more than one archive, the observation with the best statistics has been used for the data analysis and the results of the best fits are reported in Table A1.

All sources have been observed with the *Swift/X-Ray Telescope (XRT)* with the exception of PKS 0312-770, SWIFT J0709.3-1527 and SWIFT J1238.6+0928, for which *XMM–Newton* observations were available. Furthermore, 7 of the 52 AGN (PKS 0637-752, SWIFT J0845.0-3531, SWIFT J1410.9-4229, MCG-01-40-00, IGR J18308+0928, 4C +21.55 and UGC 12049) have *NuSTAR* data available although only in four sources these data are of better statistical quality than the *XRT* ones in the same energy band. In columns 6 and 7 of Table A1 the net exposure and the signal to noise ratios are listed; the exposures with no label correspond to the *XRT* data while the sources for which *XMM* or *NuSTAR* data have been used are labelled with 'X' and 'N', respectively.

All spectral fitting was performed in XSPEC v.12.8.2 using the solar abundances of Anders & Grevesse (1989). Uncertainties are listed at the 90 per cent confidence level ($\Delta\chi^2 = 2.71$ for one interesting parameter).

[1] Table A1 lists 108 entries since IGR J16058-7253 is a galaxy pair with both AGN detected in the X-ray band.
[2] All the coordinates have been taken from the NED archive.

Downloaded from https://academic.oup.com/mnras/article-abstract/460/1/19/2608998 by guest on 29 April 2020

3.1 *Swift*/XRT data

XRT data reduction was performed using the standard data pipeline package (XRTPIPELINE v. 0.13.2) in order to produce screened event files following the procedure described in Landi et al. (2010a). Due to the pointing strategy of *Swift*, short (a few ksec) repeated measurements are typically performed for each target, therefore to improve the statistical quality of the data, for those sources with more than one pointing, we performed the spectral analysis of each observation individually and then of the combined spectra. Indeed we found in most cases that spectra from individual pointings were compatible with each other within the respective uncertainties, thus justifying a combined analysis. In the case of spectral variability the single observations have been considered and compared to each other (see following sections).

The *XRT* spectral analysis of 44 sources out of 52 with no published X-ray data have been performed in the best energy range depending on the detection significance of the pointed source. As evident from the values reported in column 7 of Table A1, we do not always have sufficient statistics to investigate the spectral behaviour in the 2–10 keV energy range in depth. Therefore in order to characterize the X-ray spectra we have employed a simple power-law model absorbed by the Galactic column density and, if required, by intrinsic absorption. In a number of cases (11 sources) it was necessary to fix the photon index at the canonical value of $\Gamma = 1.7$ (Malizia et al. 2014) in order to estimate the absorption and the 2–10 keV flux. Generally the *XRT* exposures are not sufficient to detect the iron line at around 6 keV and therefore we could not investigate the presence of this important feature in the X-ray spectrum of AGN. This feature thought to be due to a fluorescence line from the K-shell of iron and produced when the nuclear continuum radiation is reprocessed by circumnuclear material, could allow us to investigate the site of reprocessing through its width and strength suggesting its origin in the outer broad line region and/or in the molecular torus.

In the following sections a few peculiar sources found when analysing the *XRT* data are discussed in more details.

3.1.1 *Galaxy pairs: ESO 328-36 and IGR J16058-7253*

ESO 328-36 is actually a pair of galaxies at $z = 0.023\,70$ very close to each other (0.8 arcmin) of which only one (ESO 328-IG 036 NED01) is an AGN classified as a Sey 1.8. Indeed *XRT*, which has an angular resolution of 18 arcsec and therefore is able to discriminate them, has detected only the Seyfert galaxy in the 2–10 keV band. Its X-ray spectrum is well fitted by a power law with $\Gamma = 1.77$ with no intrinsic absorption and a 2–10 keV flux of $\sim 7 \times 10^{-12}$ erg cm^{-2} s^{-1}. The lack of intrinsic absorption is at odds with the optical classification of the source and this discrepancy could indicate the presence of dust, possibly a bridge due to the galaxy merging, which obscures the broad lines in the optical band.

Another interesting case is the 'false' pair associated with the high-energy emitter IGR J16058-7253 which has already been highlighted as a pair of sources both detected in the X-ray band by Landi et al. (2011b). Following the optical follow-up work it has been assessed that the two AGN, LEDA 259580 and LEDA 259433, which are 3.4 arcmin apart, have different redshifts, 0.090 and 0.069, respectively, making them a pair only due to perspective. Of course with the *IBIS* angular resolution of 12 arcmin, the high-energy emission is a blending of the two galaxies and in this work we have re-analised *XRT* data in order to estimate the 20–100 keV flux of each of them extrapolating from the X-ray spectrum. The 2–10 keV spectral parameters we obtained are in good agreement with Landi et al. (2011b) and from these we have estimated a 20–100 keV flux of $\sim 10^{-11}$ erg cm^{-2} s^{-1} for LEDA 259580 and $\sim 6.5 \times 10^{-12}$ erg cm^{-2} s^{-1} for LEDA 259433.

Table 1. Swift-XRT observation of IGR J17379-5957 (ESO 139-G012).

Date	Expo (s)	σ	Γ	$F^a_{2-10\,\mathrm{keV}}$
05/04/2008	1940	24	$2.02^{+0.15}_{-0.10}$	$7.28^{+1.35}_{-0.90}$
06/03/2008	2640	11.5	$1.80^{+0.35}_{-0.38}$	$1.93^{+1.02}_{-0.59}$
07/10/2008	552	11	$2.05^{+0.30}_{-0.30}$	$5.40^{+1.79}_{-1.32}$
07/21/2008	4982	36	$1.97^{+0.08}_{-0.09}$	$6.27^{+0.46}_{-0.75}$
07/29/2008	3339	26	$1.97^{+0.12}_{-0.11}$	$4.68^{+0.87}_{-0.44}$
11/02/2008	2063	26	$1.89^{+0.12}_{-0.12}$	$8.85^{+0.91}_{-0.85}$
Mar-Oct 2013	1831	13	$1.83^{+0.21}_{-0.21}$	$2.98^{+0.52}_{-0.50}$
total[b]	17350	62	$1.80^{+0.07}_{-0.07}$	$6.02^{+0.27}_{-0.22}$

Notes. [a]in units of $\times 10^{-12}$ erg cm^{-2} s^{-1};
[b]values referred to the best-fitting model (see text).

3.1.2 *IGR J17379-5957 = ESO 139-G012*

IGR J17379-5957 is a new AGN from the last *IBIS* catalogue although it has already been reported at high energies by *Swift/BAT*. It is associated with the galaxy ESO 139-G012 at $z = 0.017\,02$, classified as a Seyfert 2 by Véron-Cetty & Véron (2010); however its optical spectrum does not extend to [O III] and H β wavelengths and the indication of its AGN nature comes from the hint of a broadened H α line (Márquez et al. 2004). In the X-ray band it has been observed by *Chandra* since ESO 139-G012 belongs to a set of AGN which have been correlated with the ultrahigh-energy cosmic rays (UHECRs) observed by the *Pierre Auger Collaboration* (Terrano, Zaw & Farrar 2012). *Chandra* observation has been performed in order to estimate the source bolometric luminosity since only an upper limit to the X-ray flux was available until recently (Zaw, Farrar & Greene 2009). Terrano et al. (2012) fitted the *Chandra* data assuming an absorbed power law which yielded a hard photon index ($\Gamma = 0.72 \pm 0.09$), a very low absorption $N_H < 8.2 \times 10^{21}$ cm^{-2} and a 2–10 keV flux of $4.7^{+0.6}_{-1.1} \times 10^{-12}$ erg cm^{-2} s^{-1}. The hardness of the X-ray spectrum and the lack of absorption could mimic a Compton thick AGN and hence a possible wrong estimate of the source bolometric luminosity.

We checked the *XRT* archive and found nine observations of ESO 139-G012, of which six have been performed in 2008 and three in 2013. We have first performed the spectral analysis of each single observation except for the three performed in 2013 which were too short and near in time and therefore have been summed in order to have enough statistics. A simple model consisting of a power law absorbed by the Galactic column density has been employed giving a good fit for each observation. No intrinsic absorption is required by the data in agreement with the *Chandra* results but we get a canonical photon index ($\Gamma \sim 1.9$) instead of the one found by Terrano et al. (2012). In Table 1 we have reported the spectral parameters obtained for each data set; it is evident that while the spectral shape does not change, this source exhibits a quite strong flux variability on short time-scales (days/months). Since the spectral shape is constant we summed together all the observations getting a good quality spectrum ($\sigma = 62$) which enabled us to better investigate the spectral behaviour of IGR J17379-5957. Indeed from the total spectrum soft excess emission below 2 keV is

Downloaded from https://academic.oup.com/mnras/article-abstract/460/1/19/2608998 by guest on 29 April 2020

evident, together with a hint of an iron line around 6.4 keV. Using the model wa(mekal+po+zga) in XSPEC, we find that our best fit ($\chi^2 = 171$, 137 d.o.f.) provides a gas temperature of 0.19 keV and a photon index of 1.8±0.07. The iron line is required by the data at >95 per cent confidence level, its energy is 6.45 keV with an equivalent width (EW) ranging from 126 to 636 eV. The lack of intrinsic absorption and X-ray flux variability are at odds with the source classification, making IGR J17379-5957 an even more interesting object. Being a variable source, it would be better to obtain the optical class and the column density measurement through simultaneous observations. Furthermore, it is possible that the source is an intermediate type 2 Sey (1.8-1.9) since a broad Hα line was detected previously. In these sources, optical flux variability can lead to a source misclassification (Trippe et al. 2010).

3.2 *XMM–Newton* data

For the four sources observed by *XMM–Newton* (MRK 1152, PKS 0312-770, SWIFT J0709.3-1527 and SWIFT J1238.6+0928) only the *pn* camera data have been considered. The data were reprocessed using the *XMM–Newton* Standard Analysis Software (SAS) version 14.0 employing the latest available calibration files following the standard procedure illustrated in e.g. Molina et al. (2009). The 0.3–10 keV energy range has been used to fit the data and in most cases the presence of a soft excess and an iron line in addition to a power law with Galactic and intrinsic absorption has been investigated. Indeed a soft excess has been detected in MRK 1152 and PKS 0312-770 (kT = 0.19 and 0.35 keV, respectively) both classified as Sey 1; also in SWIFT J1238.6+0928 associated with the Sey 2 galaxy 2MASX J12384342+0927362 we found evidence of a soft excess, but its nature deserves a deeper investigation due to the presence of the nearby cluster that could contaminate the source spectrum at soft energies (see Section 2).

3.2.1 SWIFT J0709.3-1527 = PKS 0706-15

SWIFT J0709.3-1527 is a new AGN listed in the last *IBIS* survey which has been associated with the radio source PKS 0706-15 and whose optical spectrum has been recently acquired revealing it to be a BL Lac object (Masetti et al., in preparation). Its spectral shape is consistent with a simple power law having a photon index $\Gamma = 2.31\pm0.06$ absorbed only by the Galactic column density; the fit does not require any spectral curvature intrinsic or due to local absorption as usually found in the X-ray spectra of BL Lac objects. The 2–10 keV flux is 1.36×10^{-11} erg cm^{-2} s^{-1} while at high energy it is detected by *IBIS* at 4.5σ in the 20–40 keV band with a flux of 6.8×10^{-12} erg cm^{-2} s^{-1} and has only an upper limit in the 40–100 keV range, in agreement with the steep photon index measured in the X-ray band. This source seems to be peculiar also in the radio waveband; Fig. 3 shows the NVSS contours of the source which indicate that SWIFT J0709.3-1527 is a core dominated radio source (its 5-GHz flux is 558±31 mJy); however a structure is evident at either side of the core resembling double jet emission. Of course much more sensitive radio observations are necessary in order to unveil the characteristics of this interesting BL Lac.

3.3 *NuSTAR* data

NuSTAR data sets from both focal plane modules (FPMA and FPMB) were processed with the NuSTAR–DAS software package (v.1.5.1) distributed with HEASOFT version 6.17. Event files were calibrated and cleaned with standard filtering criteria using the `nupipeline` task (version 20150316) of the NuSTAR CALDB.

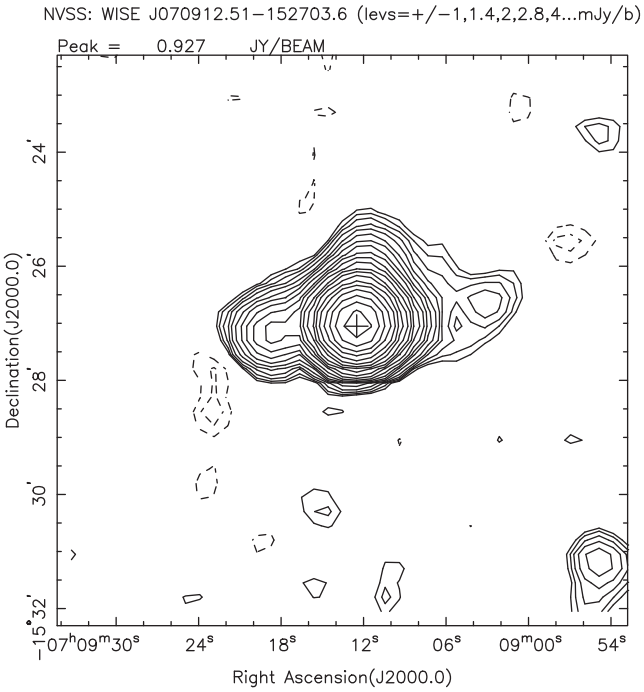

Figure 3. NVSS contours of SWIFT J0709.3-1527.

PKS 0637-752, SWIFT J0845.0-3531, SWIFT J1410.9-4229, MCG-01-40-00, IGR J18308+0928, 4C +21.55 and UGC 12049 are all well detected in the *NuSTAR* 3–78 keV energy band. The FPMA and FPMB spectra of all targets were extracted from the cleaned event files using a circle of ∼25–50 arcsec radius, depending on the source brightness, while the background was extracted from nearby circular regions of the same radius. The ancillary response files were generated with the `numkarf` task, applying corrections for the PSF losses, exposure maps and vignetting. All spectra were binned to ensure a minimum of 30 counts per bin.

Also for the *NuSTAR* data a simple power law absorbed by the Galactic column density has been first employed including a constant as a free parameter to account for cross-calibration uncertainties between the two telescopes and for all sources this was consistent with unity. Unfortunately *NuSTAR* exposures are quite short and this combined with the relatively weakness of our AGN, does not provide sufficiently high-quality spectra to allow the use of more complex spectral models. As mentioned before only the SWIFT J1410.9-4229, MCG-01-40-001, IGR J18308+0928 and UGC 12040, *NuSTAR* data were of better statistical quality than the *XRT* ones and therefore the results of this spectral analysis have been considered and reported in Table A1. However, for all the seven sources for which both *NuSTAR* and *XRT* data are available we have been able to compare the two data sets. Furthermore, since *NuSTAR* provides also high-energy (>20 keV) coverage, a comparison between 20-40 keV flux from *NuSTAR* and *INTEGRAL/IBIS* has been considered in order to have also an indication of variability at high energies. Nevertheless it is important to note that *INTEGRAL* fluxes are averaged over a long observation period while those of *NuSTAR* are single pointed observations.

3.3.1 PKS 0637-752

PKS 0637-752, classified in NED as a blazar (Flat Spectrum Radio Quasar) at $z = 0.653$, has been detected by *NuSTAR* at 25σ

Downloaded from https://academic.oup.com/mnras/article-abstract/460/1/19/2608998 by guest on 29 April 2020

signal to noise ratio versus the 65 of the *XRT* observation. The two spectra are in good agreement in their shape ($\Gamma_{NuSTAR} = 1.59\pm0.85$ and $\Gamma_{XRT} = 1.75\pm0.04$) but a significant flux variation is evident when comparing the *NuSTAR* 2–10 keV flux of 2.61×10^{-12} erg cm^{-2} s^{-1} with that of *XRT* of 4.72×10^{-12} erg cm^{-2} s^{-1}. We also found variability in the 20–40 keV band obtaining 3.4×10^{-11} erg cm^{-2} s^{-1} for *NuSTAR* and 5.3×10^{-12} erg cm^{-2} s^{-1} for *IBIS* (Bird et al. 2016). Indeed flux variability is expected for blazar objects.

3.3.2 SWIFT J0845.0-3531

For SWIFT J0845.0-3531 the two summed *XRT* observations provide higher statistical quality data than the single pointed observation of *NuSTAR*. We have analysed both data sets and found no significant flux variation in the soft (2–10) keV X-ray band, while changes in the intrinsic absorption have been detected. The best fit of the *XRT* data consists of a power law absorbed by a cold absorption of about 2×10^{22} cm^{-2} which covers 70 per cent of the central nucleus. This amount of column density does not vary in the *NuSTAR* observation ($N_H \sim 2.8 \times 10^{22}$ cm^{-2}) but the data require a total (100 per cent coverage) rather than a partial absorber. No excess around 6.4 keV is present in the *NuSTAR* data. Variable and complex absorption is often measured in broad line Seyfert like SWIFT J0845.0-3531. In these sources the absorption is likely due to ionized gas located in an accretion disc wind or in the biconical structure associated with the central nucleus (see Malizia et al. 2012 and references therein for more details). Better quality data in the soft X-ray band could provide further insight into this interesting source.

3.3.3 SWIFT J1410.9-4229

SWIFT J1410.9-4229 has recently been classified as a Seyfert 2 galaxy (Masetti et al., in preparation). *NuSTAR* best-fitting data consists of an absorbed power law with $\Gamma \sim 1.6$ and a mild column density of $N_H = 5.6 \times 10^{22}$ cm^{-2}, while the addition of an iron line does not improve the fit. Comparison in the soft X-rays with *XRT* data and at high energy with *IBIS* ones does not reveal spectral or flux variations.

3.3.4 MCG-01-40-001

MCG-01-04-001 is a Seyfert 2 galaxy whose column density measured by *NuSTAR* is quite modest ($N_H \sim 4 \times 10^{22}$ cm^{-2}). For this object we have been able to measure an iron line at 6.33 keV with an EW of 247 eV. The comparison of these data with those acquired by *XRT* is important not only because in the 0.3–2 keV range a soft excess has been detected, but mostly because a large 2–10 keV flux variation has been found: the *XRT* flux (1.04×10^{-11} erg cm^{-2} s^{-1}) is in fact more than twice that of *NuSTAR* (4.3×10^{-12} erg cm^{-2} s^{-1}). The flux variation is also found in the 20–40 keV band since *NuSTAR* measures a hard-X flux of 5.3×10^{-12} erg cm^{-2} s^{-1} while from the last *IBIS* survey we can extract a flux of 2.4×10^{-11} erg cm^{-2} s^{-1}.

3.3.5 IGR J18308+0928

IGR J18308+0928 is a Seyfert 2 galaxy for which the very low statistical quality data of *XRT* ($\sim 8\sigma$) provided us only an estimate of the 2–10 keV flux ($\sim 8 \times 10^{-13}$ erg cm^{-2} s^{-1}). The low ratio between 2–10 keV and 20–100 keV fluxes ($\sim$0.06) suggests the possibility that this could be a Compton thick AGN (Malizia et al. 2011). However, the *NuSTAR* observation provides the typical spectral shape of a Compton thin Seyfert 2 object absorbed by a column density of 12×10^{22} cm^{-2}. The source also shows an iron line at 6.31 keV with an EW of 324 eV. The 2–10 keV flux of 1.3×10^{-12} erg cm^{-2} should not be compared with the XRT one due to its low statistics, while the 20–40 keV fluxes for *NuSTAR* and *IBIS* are in agreement being both around 3×10^{-12} erg cm^{-2} s^{-1}.

3.3.6 4C +21.55

For 4C +21.55 the *XRT* data were of better statistical quality and the results of the spectral analysis are reported in the table. Furthermore, in the 0.3–2 keV *XRT* range a soft excess approximately fitted with a power law of $\Gamma = 1.97$ has been detected. *NuSTAR* data analysis gives spectral parameters in agreement with the *Swift/XRT* one; we further checked for the presence of the iron line but it is not required by the data. However, from the comparison of the two data sets flux variability is found in the 2–10 keV band ($F_{XRT} = 1.4 \times 10^{-11}$ erg cm^{-2} s^{-1} versus $F_{NuSTAR} = 7.7 \times 10^{-12}$ erg cm^{-2} s^{-1}) as well as in the 20–40 keV band ($F_{IBIS} = 1.2 \times 10^{-11}$ erg cm^{-2} s^{-1} versus $F_{NuSTAR} = 5.2 \times 10^{-12}$ erg cm^{-2} s^{-1}).

4C 21.55 is classified in the Véron-Cetty & Véron (2010) catalogue as a Sey1 and we adopted this classification since not only it is a strong radio source (5-GHz flux of almost 740 mJy), but also in the NVSS images it appears to be a classical radio galaxy with extended lobes symmetric with respect to the central source (see Bassani et al., submitted).

3.3.7 UGC 12040

UGC 12040 has comparable spectra at almost the same S/N ratio (17σ–18σ) in *NuSTAR* and *XRT* but the analysis of *NuSTAR* data allowed us to investigate the presence of the iron line. The line is required at >90 per cent significance level, is narrow, is located at 6.42±0.09 keV and has an EW of 646^{+276}_{-275} eV. Despite the large errors, the equivalent width is too large for the amount of intrinsic absorption measured ($N_H < 8 \times 10^{22}$ cm^{-2}) although better quality data are needed to assess this observational evidence. Better data are also necessary since from the comparison of our spectra flux variability is found between *NuSTAR* and *XRT* in the 2–10 keV band (1.5×10^{-12} erg cm^{-2} s^{-1} and 9×10^{-13} erg cm^{-2} s^{-1}, respectively) and mainly between *NuSTAR* and *IBIS* in the 20-40 keV range (0.8×10^{-12} erg cm^{-2} s^{-1} and 1.2×10^{-11} erg cm^{-2} s^{-1}, respectively). We note however that the *INTEGRAL* flux has large errors as UGC 12040 was detected at only 4.8σ in 20–40 keV band and has only an upper limit in the 40–100 keV band.

4 SUMMARY AND CONCLUSIONS

In this work we report new AGN detected in the last *INTEGRAL/IBIS* survey (Bird et al. 2016) which together with the large AGN sample (Malizia et al. 2012) so far detected by *INTEGRAL*, will provide a useful hard X-ray selected sample for population and correlation studies with other wavebans, even though the exposure is not uniform across the sky. To this aim we have characterized, in terms of optical class and X-ray spectral properties, all the 107 new AGN. The results are presented in this paper for the first time.

This new set of objects consists of 34 broad line or type 1 AGN (Seyfert 1-1.5), 47 narrow line or type 2 AGN (Seyfert 1.8-2) and 18 blazars. Eight sources are reported as *AGN* since their optical class

Downloaded from https://academic.oup.com/mnras/article-abstract/460/1/19/2608998 by guest on 29 April 2020

is still undetermined, while seven are considered to be good AGN candidates. Using already published X-ray data (55 AGN) or retrieving and analysing available data from *Swift/XRT*, *Newton-XMM* and *NuSTAR* archives (52 AGN), we have been able to study the X-ray spectral characteristics of all 107 new AGN. Among the seven candidates there is only one source (1RXS J112955.1-655542) which has never been observed in the X-ray band. Unfortunately the X-ray spectra are not always of good statistical quality and therefore we cannot employ sophisticated physical models; usually a power law absorbed by the Galactic column density has been employed initially and then the presence of intrinsic absorption, a soft excess below 2 keV and iron line at 6.4 keV, have been investigated. Generally we found that the majority of type 2 AGN were intrinsically absorbed while type 1 AGN are generally unobscured as expected in the simplest version of the unified model of AGN. Nevertheless even with this basic spectral analysis we have been able to identify exceptions and peculiar sources.

Among the 34 type 1 AGN, only 4 were shown to be absorbed by a column density $N_H > 10^{22}$ cm^{-2} and these 4 objects (SWIFT J0845.0-3531, IGR J14488-4008, IGR J17488-2338 and IGR J18078+1123) are all of intermediate class 1.2-1.5 where X-ray absorption is not so rare (Malizia et al. 2012).

Almost all of the 47 type 2 galaxies were absorbed by a column density $N_H > 10^{22}$ cm^{-2}, the only exceptions are: IGR J17379-5957, which is extensively discussed in Section 3.1.2, and 4 intermediate type 2 AGN. In fact, among the 11 Seyferts 1.8-1.9 studied in this work, we found four galaxies whose X-ray data do not require extra absorption, while the remaining seven are absorbed and one of them (NGC 7479) is even Compton thick. As in the case of IGR J17379-5957 (Section 3.1.2), the intermediate type 2 objects could be misclassified (Trippe et al. 2010). Furthermore, the location of the obscuring material could be another possible explanation for the discrepancy between absorbed and not absorbed intermediate type 2 AGN; in fact it is common to found bars or dust lanes in the host galaxies of these AGN. The study of the correlation between X-ray absorption and optical classification taking into account the environment of the AGN is beyond the scope of this work and will be treated in a forthcoming paper (Malizia et al., in preparation). It is worth noting that with this update of the *INTEGRAL* AGN catalogue, we find three new local Compton thick AGN (NGC 3079, NGC 6926 and NGC 7479), all already known in the literature but not detected by *INTEGRAL* before. We also point out that there is a Seyfert 2, SWIFT J0623.8-3215, which has a large column density compatible within the errors with a Compton thick AGN ($N_H = 82^{+34}_{-24} \times 10^{22}$ cm^{-2}), but the statistical quality of the *XRT* observation is too poor to draw any conclusion and a better X-ray observation is required to verify this measure. Another particular type 2 source that definitely deserves a deeper investigation is the likely Sey 2 IGR J15415-5029. Its *Chandra* observation (Tomsick et al. 2012) points to a relatively low column density ($N_H < 1.1 \times 10^{22}$ cm^{-2}), a negative photon index $\Gamma = -0.43$ and a low 2–10 keV flux ($\sim 5 \times 10^{-13}$ erg cm^{-2} s^{-1}). Due to the low *Chandra* significance detection (only 46.4 ACIS counts) it could be that the fit gives incorrect values and unfortunately also *XRT* has only one short observation detecting the source at a low signal-to-noise ratio ($<3\sigma$). However, the low flux softness ratio ($F_{(2-10)keV}/F_{(20-100)keV} = 0.05$ see Malizia et al. (2007)) could indicate the presence of a much large absorption. Therefore, this source could be considered a Compton thick candidate and its nature can be clarified only with a good quality X-ray spectrum.

Concerning the eight objects which are still optically unclassified, seven presented mild/strong absorption and so presumably are type 2 AGN, while only one does not have intrinsic absorption and so it is probably a type 1 AGN. Two of these objects are strong radio galaxies and indeed in this new set of AGN there are in total 13 radio galaxies which correspond to 12 per cent of the sample. Seven of them are giant radio galaxies (size greater than 0.7 Mpc); in particular B2 1144+35 is newly detected in the hard X-ray band. The large percentage of radio galaxies in hard X-ray selected samples of AGN is extensively discussed in Bassani et al. (submitted) where it is reported the evidence that the high-energy selection seems to favour the discovery of giant radio sources.

In this new set of *INTEGRAL* AGN there are 18 blazar (FSRQ and BL Lac) of which only 9, half of the sample, have been detected at very high energies by *Fermi*, the remaining are all compact radio sources and definitively deserve deeper investigations.

As a final remark we note that in this new set of high energy selected AGN, we found a number of sources which show flux variability. Seven objects have been observed both by *NuSTAR* and *XRT* and by comparing the results of the two data sets we found that five show 2–10 keV flux variability and three were variable also in 20–40 keV band. Finally we draw attention to the intriguing source IGR J17379-5957 for which many *XRT* observations, spanning the period 2008 and 2013, were available and which revealed a quite strong variability on time-scales of days/months.

ACKNOWLEDGEMENTS

This research has made use of data obtained from the SIMBAD data base operated at CDS, Strasbourg, France; the High Energy Astrophysics Science Archive Research Center (HEASARC), provided by NASA's Goddard Space Flight Center NASA/IPAC Extragalactic Database (NED). The authors acknowledge the ASI financial support via ASI–INAF grant 2013-025-R.0.

REFERENCES

Abdo A. A. et al., 2010, ApJ, 716, 835
Anders E., Grevesse N., 1989, Geochim. Cosmochim. Acta, 53, 197
Ballo L., Severgnini P., Braito V., Campana S., Della Ceca R., Moretti A., Vignali C., 2015, A&A, 581, A87
Barrière N. M., Tomsick J. A., Wik D. R., Chaty S., Rodriguez J., 2015, ApJ, 799, 24
Barthelmy S. D. et al., 2005, Space Sci. Rev., 120, 143
Bassani L. et al., 2005, ApJ, 634, L21
Bassani L. et al., 2009, MNRAS, 395, L1
Bassani L. et al., 2012, A&A, 543, A1
Bassani L., Landi R., Malizia A., Stephen J. B., Bazzano A., Bird A. J., Ubertini P., 2014, A&A, 561, A108
Baumgartner W. H., Tueller J., Markwardt C. B., Skinner G. K., Barthelmy S., Mushotzky R. F., Evans P. A., Gehrels N., 2013, ApJS, 207, 19
Bird A. J. et al., 2016, ApJS, 223, 15
Blustin A. J., Page M. J., Branduardi-Raymont G., 2004, A&A, 417, 61
Bozzo E., Pavan L., Ferrigno C., Falanga M., Campana S., Paltani S., Stella L., Walter R., 2012, A&A, 544, A118
Brightman M., Nandra K., 2011, MNRAS, 413, 1206
Cardaci M. V., Santos-Lleó M., Hägele G. F., Krongold Y., Díaz A. I., Rodríguez-Pascual P., 2011, A&A, 530, A125
Castangia P., Panessa F., Henkel C., Kadler M., Tarchi A., 2013, MNRAS, 436, 3388
Donato D., Sambruna R. M., Gliozzi M., 2005, A&A, 433, 1163
Edelson R., Malkan M., 2012, ApJ, 751, 52
Eguchi S., Ueda Y., Terashima Y., Mushotzky R., Tueller J., 2009, ApJ, 696, 1657
Evans D. A., Hardcastle M. J., Lee J. C., Kraft R. P., Worrall D. M., Birkinshaw M., Croston J. H., 2008, ApJ, 688, 844

Downloaded from https://academic.oup.com/mnras/article-abstract/460/1/19/2608998 by guest on 29 April 2020

Ghisellini G., Tavecchio F., Ghirlanda G., 2009, MNRAS, 399, 2041
Greenhill L. J., Tilak A., Madejski G., 2008, ApJ, 686, L13
Iwasawa K., Lee J. C., Young A. J., Reynolds C. S., Fabian A. C., 2004, MNRAS, 347, 411
Iyomoto N., Fukazawa Y., Nakai N., Ishihara Y., 2001, ApJ, 561, L69
Landi R. et al., 2007, ApJ, 669, 109
Landi R. et al., 2009, A&A, 493, 893
Landi R., Bassani L., Malizia A., Stephen J. B., Bazzano A., Fiocchi M., Bird A. J., 2010a, MNRAS, 403, 945
Landi R. et al., 2010b, Astron. Telegram, 2853, 1
Landi R., Malizia A., Bazzano A., Fiocchi M., Bird A. J., Gehrels N., 2011a, Astron. Telegram, 3178, 1
Landi R., Bassani L., Masetti N., Bazzano A., Bird A. J., 2011b, Astron. Telegram, 3271, 1
Landi R., Bassani L., Bazzano A., Fiocchi M., Bird A. J., 2013, preprint (arXiv:1304.4405)
Maiorano E. et al., 2011, MNRAS, 416, 531
Malizia A. et al., 2007, ApJ, 668, 81
Malizia A., Bassani L., Sguera V., Stephen J. B., Bazzano A., Fiocchi M., Bird A. J., 2010, MNRAS, 408, 975
Malizia A., Landi R., Bazzano A., Bird A. J., Gehrels N., Kennea J. A., 2011, Astron. Telegram, 3391, 1
Malizia A., Bassani L., Bazzano A., Bird A. J., Masetti N., Panessa F., Stephen J. B., Ubertini P., 2012, MNRAS, 426, 1750
Malizia A., Molina M., Bassani L., Stephen J. B., Bazzano A., Ubertini P., Bird A. J., 2014, ApJ, 782, L25
Márquez I. et al., 2004, A&A, 416, 475
Masetti N. et al., 2013, A&A, 556, A120
Matt G., Bianchi S., Awaki H., Comastri A., Guainazzi M., Iwasawa K., Jimenez-Bailon E., Nicastro F., 2009, A&A, 496, 653
Mingo B., Hardcastle M. J., Croston J. H., Dicken D., Evans D. A., Morganti R., Tadhunter C., 2014, MNRAS, 440, 269
Molina M. et al., 2009, MNRAS, 399, 1293
Molina M., Landi R., Bassani L., Malizia A., Stephen J. B., Bazzano A., Bird A. J., Gehrels N., 2012, A&A, 548, A32
Molina M., Bassani L., Malizia A., Bird A. J., Bazzano A., Ubertini P., Venturi T., 2014, A&A, 565, A2
Molina M., Venturi T., Malizia A., Bassani L., Dallacasa D., Lal D. V., Bird A. J., Ubertini P., 2015, MNRAS, 451, 2370
Parisi P. et al., 2012, A&A, 545, A101
Ricci C., Bozzo E., Walter R., Paltani S., Stella L., 2012, Astron. Telegram, 4102, 1
Sazonov S., Revnivtsev M., Burenin R., Churazov E., Sunyaev R., Forman W. R., Murray S. S., 2008, A&A, 487, 509
Shinozaki K., Miyaji T., Ishisaki Y., Ueda Y., Ogasaka Y., 2006, AJ, 131, 2843
Shu X. W., Wang J. X., Jiang P., Fan L. L., Wang T. G., 2007, ApJ, 657, 167
Tavecchio F., Becerra-Gonzalez J., Ghisellini G., Stamerra A., Bonnoli G., Foschini L., Maraschi L., 2011, A&A, 534, A86
Terrano W. A., Zaw I., Farrar G. R., 2012, ApJ, 754, 142
Tombesi F., Cappi M., Reeves J. N., Palumbo G. G. C., Yaqoob T., Braito V., Dadina M., 2010, A&A, 521, A57
Tomsick J. A., Bodaghee A., Chaty S., Rodriguez J., Rahoui F., Halpern J., Kalemci E., Özbey Arabaci M., 2012, ApJ, 754, 145
Trippe M. L., Crenshaw D. M., Deo R. P., Dietrich M., Kraemer S. B., Rafter S. E., Turner T. J., 2010, ApJ, 725, 1749
Ubertini P. et al., 2003, A&A, 411, L131
Vasudevan R. V., Brandt W. N., Mushotzky R. F., Winter L. M., Baumgartner W. H., Shimizu T. T., Schneider D. P., Nousek J., 2013, ApJ, 763, 111
Véron-Cetty M.-P., Véron P., 2010, A&A, 518, A10
Winter L. M., Mushotzky R. F., Reynolds C. S., Tueller J., 2009, ApJ, 690, 1322
Winter L. M., Veilleux S., McKernan B., Kallman T. R., 2012, ApJ, 745, 107
Zaw I., Farrar G. R., Greene J. E., 2009, ApJ, 696, 1218

APPENDIX A: LIST OF THE NEW AGN

Table A1 lists all the new 107 AGN and, at the end, 7 sources which we consider to be good AGN candidates. In column 2 are listed alternative names present in previous catalogues. Coordinates, redshift and class are reported in columns from 3 to 6. In column 7 are listed the satellites used to acquired X-ray data for the 55 sources already known in the literature or XRT/*XMM*/NuSTAR net exposures for data analysed in this work. For the sources analysed here, XRT detection significance in the 0.3–10 keV band is reported in column 8. Intrinsic absorption, photon index and 2–10 keV flux are listed in columns 9, 10, 11 respectively, while the 20–100 keV fluxes extracted from Bird et al. (2016) are reported in column 12. Finally in column 13, references for the X-ray spectral parameters are listed.

Table A1. *INTEGRAL*/IBIS AGN.

Name	Prev. cat name	RA	Dec	z	Class	Exp/instr.	σ	$N_H{}^a$	Γ	F_S^b	F_H^c	REF
SWIFT J0034.5-7904	1RXS J003422.2-790525	00 34 16.7	−79 05 20	0.074 00	Sy1	10500	65	–	$2.24^{+0.04}_{-0.04}$	6.33	1.09	1
Mrk 352		00 59 53.3	+31 49 37	0.014 86	Sy1	*XMM*	–	–	$1.70^{+0.02}_{-0.01}$	11.89	3.21	2
Mrk 1152		01 13 50.1	−14 50 44	0.052 71	Sy1.5	19560[d]	209	–	$1.61^{+0.02}_{-0.02}$	4.66	2.94	1
Fairall 9		01 23 45.8	−58 48 21	0.047 02	Sy1.2	*XMM*	–	–	$1.64^{+0.03}_{-0.03}$	7.40	3.34	3
IGR J01528-0845	2MASX J01524845-0843202	01 52 48.4	−08 43 21	0.036 97	Sy2[e]	14080	6	30.9^{+73}_{-19}	$1.93^{+1.5}_{-1.5}$	0.40	0.85	1
Mrk 584		02 00 26.3	+02 40 10	0.078 77	Sy1.8	9560	47	–	$2.13^{+0.07}_{-0.07}$	3.98	1.79	1
IGR J02341+0228	QSO B0231+022	02 33 49.0	+02 29 25	0.321 00	QSO	XRT	–	–	$2.10^{+0.30}_{-0.30}$	2.90	1.55	4
SWIFT J0249.1+2627	2MASX J02485937+2630391	02 48 59.3	+26 30 39	0.058 00	Sy2	8706	12	$27.1^{+10.1}_{-7.1}$	1.7 fixed	3.73	1.90	1
MCG-02-08-038		03 00 04.3	−10 49 29	0.032 59	Sy1	3961	38	$0.36^{+0.27}_{-0.27}$	$1.60^{+0.20}_{-0.20}$	16.7	1.81	1
PKS 0312-770		03 11 55.2	−76 51 51	0.225 19	Sy1/QSO	23562[d]	153	–	$1.67^{+0.06}_{-0.06}$	2.19	1.21	1
SWIFT J0353.7+3711	2MASX J03534246+3714077	03 53 42.5	+37 14 07	0.018 65	Sy2/Liner	XRT	–	$3.7^{+2.0}_{-1.7}$	$1.71^{+0.59}_{-0.55}$	3.50	0.89	5
4C +62.08[f]		03 55 40.2	+62 40 59	1.109 00	Sy1	7614	7	–	$1.47^{+0.60}_{-0.60}$	0.45	1.30	1

Downloaded from https://academic.oup.com/mnras/article-abstract/460/1/19/2608998 by guest on 29 April 2020

Table A1. *– continued*

Name	Prev. cat name	RA	Dec	z	Class	Exp/instr.	σ	N_H[a]	Γ	F_S^b	F_H^c	REF
SWIFT J0357.6+4153	2MASX J03574513+4155049	03 57 45.1	+41 55 05	0.053 00	Sy1.9[e]	10800	25	$2^{+0.7}_{-0.6}$	$1.61^{+0.04}_{-0.04}$	5.88	1.55	1
SWIFT J0444.1+2813	2MASX J04440903+2813003	04 44 09.0	+28 13 01	0.011 27	Sy2	XRT	–	$3.39^{+0.31}_{-0.25}$	$1.37^{+0.11}_{-0.08}$	12.34	1.49	2
SWIFT J0450.7-5813	2MASX J04514402-5811005	04 51 44.0	−58 11 01	0.090 70	Sy1.5	12000	34	$0.09^{+0.04}_{-0.03}$	$1.45^{+0.13}_{-0.13}$	4.74	1.85	1
MCG -01-13-025		04 51 41.5	−03 48 33	0.015 89	Sy1.2	*XMM*	–	–	$1.70^{+0.03}_{-0.03}$	21.3	1.47	2
IGR J05081+1722	2MASX J05081967+1721483	05 08 19.7	+17 21 48	0.017 50	Sy2	XRT	–	$2.40^{+0.30}_{-0.30}$	$1.80^{+0.10}_{-0.10}$	6.45	1.25	6
SWIFT J0515.3+1854	2MASX J05151978+1854515	05 15 19.8	+18 54 52	0.023 49	Sy2	7956	8	$11.6^{+8.6}_{-4.4}$	1.7 fixed	1.91	1.81	1
SWIFT J0516.3+1928	2MFGC 04298	05 16 22.7	+19 27 11	0.021 15	Sy2	7879	10	$4.4^{+2.4}_{-1.3}$	1.7 fixed	1.80	1.53	1
SWIFT J0544.4+5909	2MASX J05442257+5907361	05 44 22.6	+59 07 36	0.065 97	Sy1.9	33800	45	$1.83^{+0.3}_{-0.3}$	$1.62^{+0.18}_{-0.18}$	5.25	2.00	1
IGR J05470+5034	2MASX J05471492+5038251	05 47 14.9	+50 38 25	0.036 00	Sy2	17500	11	15^{+16}_{-9}	$1.60^{+1.60}_{-0.90}$	1.40	1.19	1
SWIFT J0623.8-3215	ESO 426−G 002	06 23 46.4	−32 13 00	0.022 43	Sy2	31300	10	82^{+34}_{-24}	1.7 fixed	1.16	1.94	1
PKS 0637-752		06 35 46.5	−75 16 17	0.653 00	QSO/blazar	27100	65	–	$1.75^{+0.04}_{-0.04}$	4.72	1.66	1
SWIFT J0709.3-1527	PKS 0706-15	07 09 12.3	−15 27 00	0.139 00	BL Lac[e]	606[d]	55	–	$2.31^{+0.06}_{-0.06}$	13.6	<1.25	1
IGR J07225-3810[f]	PMN J0722-3814	07 22 22.4	−38 14 55	1.023	QSO/blazar[e]	XRT	–	–	$1.52^{+0.45}_{-0.46}$	0.58	2.08	7
PKS 0723-008		07 25 50.6	−00 54 57	0.128 00	BL Lac	29700	62	–	$1.54^{+0.09}_{-0.11}$	4.97	1.58	1
Mrk 79		07 42 32.8	+49 48 35	0.022 19	Sy1.2	Suzaku	–	–	$1.51^{+0.40}_{-0.04}$	15.8	4.89	8
Mrk 1210		08 04 05.8	+05 06 50	0.013 50	Sy2	Suzaku	–	$33^{+2.2}_{-2.2}$	$1.87^{+0.23}_{-0.18}$	9.70	5.96	9
SWIFT J0845.0-3531	1RXS J084521.7-353048	08 45 21.4	−35 30 24	0.137 00	Sy1.2	15400	34	$2.4^{+0.88}_{-0.88}$	$1.83^{+0.31}_{-0.33}$	4.64	1.11	1
Mrk 18		09 01 58.4	+60 09 06	0.011 09	Sy2	*XMM*	–	$18.25^{3.6}_{-2.7}$	$1.62^{+0.31}_{-0.22}$	1.57	2.62	2
1RXS J090431.1-382920		09 04 33.3	−38 29 22	0.016 03	Sy1	4657	8.4	–	$1.35^{+0.38}_{-0.38}$	0.92	0.92	1
IGR J09189-4418[f]	2MASX J09185877-4418302	09 18 58.8	−44 18 30	–	AGN	*Chandra*	–	$4.6^{+1.1}_{-1.3}$	$1.4^{+0.4}_{-0.4}$	2.30	0.53	10
SWIFT J0929.7+6232	CGCG 312-012	09 29 37.8	+62 32 39	0.025 61	Sy2	10310	7	$20.5^{+23.8}_{-12.3}$	1.7 fixed	0.97	2.06	1
4C 73.08		09 49 45.8	+73 14 23	0.058 10	Sy2	*XMM*	–	92^{+54}_{-29}	1.7 fixed	1.81	1.17	11
M 81		09 55 33.2	+69 03 55	0.000 84	Sy1.8/Liner	*XMM*	–	–	$1.83^{+0.03}_{-0.02}$	11.1	1.11	12
SWIFT J0959.7-3112	2MASX J09594263-3112581	09 59 42.6	−31 12 58	0.037 00	Sy1	13200	69	–	$2.23^{+0.04}_{-0.04}$	7.18	2.21	1
NGC 3079		10 01 57.8	+55 40 47	0.003 72	Sy2	BeppoSAX	–	1000^{+1140}_{-530}	1.9 fixed	38.0	3.72	13
SWIFT J1143.7+7942	UGC 06728	11 45 16.0	+79 40 53	0.006 52	Sy1.2	*XMM*	–	$0.01^{+0.01}_{-0.01}$	$1.78^{+0.03}_{-0.02}$	6.51	2.21	2
B2 1144+35B		11 47 22.1	+35 01 08	0.063 13	Sy1.9[e]	4772	20	–	$1.66^{+0.14}_{-0.14}$	3.09	1.21	1
Mrk 198		12 09 14.1	+47 03 30	0.024 22	Sy2	*XMM*	–	$10^{+0.1}_{-0.1}$	$1.61^{+0.04}_{-0.04}$	5.12	1.09	14
PKS 1217+02		12 20 11.9	+02 03 42	0.240 23	Sy1.2	14500	55	–	$1.99^{+0.05}_{-0.05}$	4.38	1.02	1
PG 1218+305		12 21 21.9	+30 10 37	0.183 65	BL Lac	*XMM*	–	–	$2.61^{+0.02}_{-0.02}$	0.26	0.92	15
PG 1222+216		12 24 54.4	+21 22 46	0.432 00	QSO/blazar	XRT	–	–	$2.12^{+0.14}_{-0.14}$	8.30	1.64	16
IGR J12319-0749[f]	1RXS J123158.3-074705	12 31 57.7	−07 47 18	3.668 00	QSO/blazar	XRT	–	–	$0.96^{+0.33}_{-0.33}$	5.70	0.98	17
Mrk 771		12 32 03.6	+20 09 29	0.063 01	Sy1	*XMM*	–	–	$2.14^{+0.03}_{-0.02}$	3.01	0.83	14
XSS J12303-4232	1RXS J123212.3-421745	12 32 11.8	−42 17 52	0.100 00	Sy1.5	XRT	–	–	$1.76^{+0.03}_{-0.04}$	5.40	1.36	18
SWIFT J1238.6+0928	2MASX J12384342+0927362	12 38 43.4	+09 27 37	0.082 90	Sy2	16590[d]	37	$32.9^{+3.7}_{-3.3}$	$2.3^{+0.17}_{-0.16}$	0.92	0.58	1
IGR J13107-5626[f]	2MASX J13103701-5626551	13 10 37.0	−56 26 55	–	AGN/RG	XRT	–	$39.3^{+24.4}_{-13.3}$	1.8 fixed	1.10	1.02	19
IGR J13133-1109	PG 1310-108	13 13 05.8	−11 07 42	0.034 27	Sy1	11400	67	–	$1.87^{+0.10}_{-0.11}$	8.0	1.34	1
NGC 5100		13 20 58.6	+08 58 55	0.031 90	Liner	XRT	–	$14.45^{+1.41}_{-1.44}$	$2.02^{+0.14}_{-0.13}$	4.35	1.38	14
SWIFT J1344.7+1934	CGCG 102-048	13 44 15.6	+19 34 00	0.027 06	Sy2/Liner	13330	5	24.6^{+15}_{-9}	1.7 fixed	0.44	1.98	1
IGR J13477-4210	ESO 325-IG 022	13 48 15.2	−42 10 20	0.038 60	Sy2	5045	6	$6.25^{+5.3}_{-3.0}$	1.7 fixed	1.19	<0.83	1
PKS 1355-416		13 59 00.2	−41 52 53	0.313 00	Sy1	*XMM*	–	$0.27^{+0.24}_{-0.18}$	1.7 fixed	1.16	0.75	20
SWIFT J1410.9-4229	2MASX J14104482-4228325	14 10 44.8	−42 28 33	0.033 94	Sy2[e]	22230[g]	28	$5.7^{+3.4}_{-3.1}$	$1.57^{+0.14}_{-0.13}$	2.07	1.02	1
SWIFT J1417.7+2539	1RXS J141756.8+254329	14 17 56.7	+25 43 26	0.237 00	BL Lac	14600	84	–	$2.07^{+0.03}_{-0.03}$	12.0	2.17	1
NGC 5674		14 33 52.2	+05 27 30	0.024 93	Sy1.9	XRT	–	$11.2^{+6.1}_{-2.7}$	$2.14^{+0.06}_{-0.25}$	4.85	1.81	14
SWIFT J1436.8-1615	2MASX J14364961-1613410	14 36 49.6	−16 13 41	0.144 54	Sey1/QSO	9400	45	–	$1.72^{+0.06}_{-0.06}$	7.19	2.00	1
IGR J14488-4008[f]	WISE J144850.99-400845.6	14 48 51.0	−40 08 46	0.123 00	Sy1.2	*XMM*	–	$7.85^{+3.04}_{-2.37}$	$1.71^{+0.16}_{-0.17}$	5.27	0.75	21
IGR J14492-5535[f]	CXO J144917.3-553544	14 49 17.3	−55 35 45	–	AGN	*Chandra*	–	12	1.8 fixed	3.10	1.81	22
PKS 1451-375		14 54 27.4	−37 47 33	0.314 05	Sy1.2	1643	12.5	–	$1.74^{+0.27}_{-0.27}$	3.18	0.98	1
1RXS J150101.7+223812		15 01 01.8	+22 38 06	0.235 00	BL Lac	BeppoSAX	–	–	$2.62^{+0.23}_{-0.12}$	0.70	3.69	23

Downloaded from https://academic.oup.com/mnras/article-abstract/460/1/19/2608998 by guest on 29 April 2020

Table A1. *– continued*

Name	Prev. cat name	RA	Dec	z	Class	Exp/instr.	σ	N_H[a]	Γ	F_S^b	F_H^c	REF
SWIFT J1508.6-4953	1RXS J150839.0-495304	15 08 39.0	−49 53 02	–	Blazar	XRT	–	–	$1.41^{+0.10}_{-0.10}$	2.80	0.96	24
PKS 1510-089		15 12 50.5	−09 06 00	0.360 00	QSO/blazar	Suzaku	–	–	$1.37^{+0.01}_{-0.01}$	6.31	3.85	25
ESO 328-36		15 14 47.2	−40 21 35	0.023 70	Sy1.8	10500	15	–	$1.77^{+0.21}_{-0.21}$	7.13	0.85	1
IGR J15301-3840	ESO 329- G 007	15 30 08.0	−38 39 07	0.015 53	Sy2[e]	3099	9.8	$2.27^{+1.96}_{-1.36}$	$1.74^{+1.30}_{-1.07}$	3.34	0.77	1
MCG-01-40-001		15 33 20.7	−08 42 02	0.022 71	Sy2	21640[g]	45	$3.9^{+1.95}_{-1.83}$	$1.54^{+0.09}_{-0.08}$	4.27	1.77	1
IGR J15359-5750[f]	CXO J153602.7-574853	15 36 02.8	−57 48 53	–	AGN	*XMM*	–	$20.1^{+2.5}_{-2.9}$	$1.85^{+0.27}_{-0.25}$	4.97	2.06	26
IGR J15415-5029[f]	WKK 5204	15 41 26.4	−50 28 23	0.032 00	Sy2?	*Chandra*	–	<1.1	$-0.43^{+0.68}_{-0.44}$	0.54	1.04	10
IGR J16058-7253 (1)	LEDA 259580	16 06 06.9	−72 52 42	0.090 00	Sy2	25200	8	$37.9^{+10.9}_{-15.8}$	$1.75^{+1.55}_{-1.64}$	3.18	0.90	1
IGR J16058-7253 (2)	LEDA 259433	16 05 23.2	−72 53 56	0.069 00	Sy2?	25200	15	17.4^{+6}_{-5}	$1.90^{+0.87}_{-0.49}$	3.50	0.60	1
Mrk 1498		16 28 04.0	+51 46 31	0.054 70	Sy1.9	Suzaku	–	58^{+11}_{-11}	$1.80^{+0.03}_{-0.03}$	9.00	5.09	27
SWIFT J1630.5+3925	2MASX J16303265+3923031	16 30 32.6	+39 23 03	0.030 56	Sy2	*XMM*	–	40^{+5}_{-7}	$1.20^{+0.3}_{-0.4}$	1.25	1.59	29
IGR J17111+3910	2MASX J17110531+3908488	17 11 05.3	+39 08 49	–	AGN	4922	16	–	$1.96^{+0.17}_{-0.17}$	1.47	0.96	1
IGR J17204-3554[f]		17 20 21.6	−35 54 32	–	AGN	XRT	–	16^{+3}_{-3}	$1.6^{+0.4}_{-0.4}$	2.50	1.15	28
Mrk 506		17 22 39.9	+30 52 53	0.043 03	Sy1.5	ASCA	–	<0.05	$1.93^{+0.07}_{-0.05}$	6.30	1.81	30
SWIFT J1723.5+3630	2MASX J17232321+3630097	17 23 23.2	+36 30 10	0.040 00	Sy1.5	8745	40	$0.19^{+0.06}_{-0.05}$	$1.56^{+0.11}_{-0.11}$	8.39	1.79	1
PKS 1730-13		17 33 02.7	−13 04 50	0.902 00	QSO/blazar	40800	34	$0.87^{+0.09}_{-0.08}$	$1.61^{+0.15}_{-0.15}$	1.46	1.30	1
IGR J17348-2045[f]	NVSS J173459-204533	17 34 59.1	−20 45 34	0.044	Sy2[e]	*XMM*	–	17^{+7}_{-5}	$1.5^{+0.8}_{-0.7}$	2.2	1.7	31
IGR J17379-5957	ESO 139- G 012	17 37 39.1	−59 56 27	0.017 02	Sy2	17400	61	–	$1.80^{+0.07}_{-0.07}$	6.02	1.17	1
PKS 1741-03		17 43 58.8	−03 50 05	1.054 00	QSO/blazar	19800	25	–	$1.35^{+0.19}_{-0.18}$	2.09	0.70	1
IGR J17448-3232[f]	CXOU J174453.4-323254	17 44 55.0	−32 32 00	0.055 00	Cluster/blazar	*XMM*	–	$2.51^{+0.25}_{-0.23}$	$1.31^{+0.09}_{-0.09}$	1.65	1.11	32
IGR J17488-2338[f]		17 48 39.0	−23 35 21	0.240 00	Sy1.5	*XMM*	–	$1.14^{+0.26}_{-0.23}$	$1.37^{+0.11}_{-0.11}$	2.0	1.58	33
IGR J17520-6018[f]	2MASX J17515581-6019430	17 51 55.8	−60 19 43	0.112 00	Sy2	XRT	–	13	1.8 fixed	2.55	2.19	34
NGC 6552		18 00 07.2	+66 36 54	0.026 49	Sy2	*XMM*	–	71^{+40}_{-10}	$2.85^{+0.37}_{-0.13}$	0.43	0.85	35
IGR J18078+1123	2MASX J18074992+1120494	18 07 49.9	+11 20 49	0.078 00	Sy1.2	17200	52	$1.79^{+0.47}_{-0.42}$	$2.00^{+0.19}_{-0.20}$	6.32	1.26	1
IGR J18129-0649[f]	PMN J1812-0648	18 12 50.9	−06 48 24	0.775 00	Sy1/QSO[e]	XRT	–	–	$1.44^{+0.41}_{-0.43}$	2.74	0.66	7
SWIFT J1821.6+5953	2MASX J18212680+5955209	18 21 26.8	+59 55 21	0.0990	Sy2	10500	11	$7.65^{+3.7}_{-2.3}$	1.7 fixed	1.49	1.41	1
IGR J18308+0928[f]	2MASX J18305065+0928414	18 30 50.6	+09 28 42	0.019 00	Sy2	22720[g]	24	$11.9^{+7.8}_{-6.5}$	$1.54^{+0.27}_{-0.24}$	1.30	1.32	1
Fairall 49		18 36 58.3	−59 24 09	0.020 02	Sy2	*XMM*	–	$1.24^{+0.08}_{-0.11}$	$2.06^{+0.03}_{-0.03}$	12.0	1.51	36
SWIFT J1845.4+7211	CGCG 341-006	18 45 26.2	+72 11 02	0.046 30	Sy2	11290	18.5	$3.24^{+0.57}_{-0.46}$	1.7 fixed	4.22	1.00	1
PBC J1850.7-1658	PMN J1850-1655	18 50 51.6	−16 55 58	–	AGN/RG	4295	10.5	$1.49^{+0.62}_{-0.44}$	1.7 fixed	2.19	1.28	1
IGR J18538-0102[f]	2XMM J185348.4-010229	18 53 48.4	−01 02 30	0.145 00	Sy1	*XMM*	–	$0.41^{+0.1}_{-0.1}$	$1.56^{+0.08}_{-0.08}$	4.0	1.02	26
SWIFT J1933.9+3258	2MASS J19334715+3254259	19 33 47.1	+32 54 26	0.0565	Sy1.2	XRT	–	<0.04	$2.08^{+0.05}_{-0.04}$	13.8	1.30	18
IGR J19443+2117[f]	2MASS J19435624+2118233	19 43 56.2	+21 18 23	–	BL Lac?	XRT	–	$0.54^{+0.12}_{-0.13}$	$2.04^{+0.12}_{-0.12}$	18.3	1.00	37
1ES 1959+650		19 59 59.8	+65 08 55	0.047 00	BL Lac	XRT	–	$0.07^{+0.04}_{-0.04}$	$1.93^{+0.11}_{-0.10}$	91.7	1.57	2
SWIFT J2018.4-5539	PKS 2014-55	20 18 01.3	−55 39 31	0.060 63	Sy2	10800	13	$31.4^{+11.6}_{-9}$	1.7 fixed	4.01	3.64	1
IGR J20159+3713	LEDA 101342	20 15 28.8	+37 11 00	0.857	QSO/blazar[e, h]	XRT	–	$0.78^{+0.33}_{-0.29}$	$1.66^{+0.22}_{-0.20}$	2-5 (var)	1.11	38
NGC 6926		20 33 06.1	−02 01 39	0.019 61	Sy2	*XMM*	–	100	1.7 fixed	0.07	1.36	39
4C +21.55		20 33 32.0	+21 46 22	0.173 50	Sey1	19800	75	$0.60^{+0.42}_{-0.20}$	$1.68^{+0.50}_{-0.11}$	14.0	2.91	1
IGR J21178+5139[f]	2MASX J21174741+5138523	21 17 47.2	+51 38 54	–	AGN	XRT	–	$2.11^{+1.52}_{-1.03}$	1.8 fixed	2.1	1.81	40
CTS 109		21 32 02.1	−33 42 54	0.029 97	Sy1.2	*XMM*	–	–	$1.55^{+0.02}_{-0.02}$	7.6	1.98	41
SWIFT J2156.2+1724	2MASX J21561518+1722525	21 56 15.2	+17 22 53	0.034 00	Sy1.8[e]	8456	9	$21.5^{+37.5}_{-9.83}$	1.7 fixed	1.77	2.00	1
UGC 12040		22 27 05.8	+36 21 42	0.021 33	Sy1.9	21340[g]	17	< 8.3	$1.63^{+0.29}_{-0.19}$	0.86	2.62	1
KAZ 320		22 59 32.9	+24 55 06	0.034 50	NLSy1	7305	52	–	$1.91^{+0.05}_{-0.05}$	10.1	1.49	1
NGC 7479		23 04 56.6	+12 19 22	0.007 94	Sy1.9	*XMM*	–	201^{+493}_{-122}	1.9 fixed	0.33	1.40	13
RHS 61		23 25 54.2	+21 53 14	0.120 00	Sy1	3414	24	–	$1.86^{+0.11}_{-0.11}$	4.32	1.43	1
PKS 2325+093		23 27 33.6	+09 40 09	1.843 00	QSO/blazar	XRT	–	–	$1.11^{+0.17}_{-0.17}$	2.9	2.45	42
IGR J23558-1047[f]	1WGA J2355.9-1045	23 55 59.3	−10 46 45	1.108 00	Sy1/QSO	XRT	–	–	$1.97^{+0.80}_{-0.69}$	0.08	5.26	43

Downloaded from https://academic.oup.com/mnras/article-abstract/460/1/19/2608998 by guest on 29 April 2020

Table A1. – *continued*

Name	Prev. cat name	RA	Dec	z	Class	Exp/instr.	σ	$N_H{}^a$	Γ	F_S^b	F_H^c	REF
AGN CANDIDATES												
Name	Prev. cat name	RA	Dec	z	Class	Exp/instr.	σ	$N_H{}^a$	Γ	F_S^b	F_H^c	REF
IGR J02447+7046[f]i	NVSS J024443+704946	02 44 23.7	+70 29 05	–	cand	4488	4.4	–	1.7 fixed	0.18	0.96	1
IGR J02447+7046[f]i		02 43 43.0	+70 50 38	0.306 00	Sy 1.2	4488	4	–	1.7 fixed	0.13	0.96	1
RXS J112955.1-655542		11 29 55.1	−65 55 42	–	cand	–	–	–	–	–	0.94	44
IGR J14466-3352[f]	NVSS J144637-335234	14 46 37.4	−33 52 34	–	cand	XRT		–	1.8 fixed	0.07	0.79	45
IGR J16413-4046[f]	CXOU J164119.4-404737	16 41 19.5	−40 47 38	–	cand	XRT	–	10	1.8 fixed	1.40	1.45	46
IGR J16560-4958[f]	CXOU J165551.9-495732	16 55 51.9	−49 57 32	–	cand	*Chandra*	–	$2.3^{+0.7}_{-0.4}$	$2.2^{+0.5}_{-0.4}$	17.0	1.10	47
AX J183039-1002[f]		18 30 38.3	−10 00 25	–	cand	*Chandra*	–	$11.4^{+3.8}_{-2.9}$	$1.01^{+0.57}_{-0.38}$	3.3	0.73	48
IGR J20569+4940[f]	MG4 J205647+4938	20 56 42.7	+49 40 07	–	cand	XRT	–	$0.53^{+0.18}_{-0.16}$	$2.32^{+0.18}_{-0.17}$	1.19	0.83	49

Notes. [a]intrinsic column density in unit of 10^{22} cm^{-2}; [b]2–10 keV flux in units of 10^{-12} erg cm^{-2} s^{-1}; [c]20–100 keV flux in units of 10^{-11} erg cm^{-2} s^{-1}. [d]*XMM* data; [g]NuSTAR data, [(e)]new classification in Masetti et al. (in preparation); [h]: the blazar object is blended with a CV but Bassani et al. (2014) have estimated that the 90 per cent hard X-ray fluxed comes from the AGN; [i]: two X-ray sources, 1 identified as a Sy 1.2 and 1 AGN candidate, are present in the IBIS error box; References: (1): spectral analysis performed in this work; (2): Winter et al. (2009); (3) Tombesi et al. (2010); (4): Ricci et al. (2012); (5) Parisi et al. (2012); (6) Ballo et al. (2015); (7) Molina et al. (2012); (8) Winter et al. (2012); (9): Matt et al. (2009); (10): Tomsick et al. (2012); (11): Evans et al. (2008); (12): Brightman & Nandra (2011); (13): Iyomoto et al. (2001); (14): Vasudevan et al. (2013); (15): Blustin, Page & Branduardi-Raymont (2004); (16): Tavecchio et al. (2011); (17): Bassani et al. (2012); (18): Landi et al. (2007); (19) Landi et al. (2010a); (20) Mingo et al. (2014); (21): Molina et al. (2015); (22): Sazonov et al. (2008); (23): Donato, Sambruna & Gliozzi (2005); (24): Landi et al. (2013); (25): Abdo et al. (2010); (26): Malizia et al. (2010); (27): Eguchi et al. (2009); (28): Castangia et al. (2013); (29): Bassani et al. (2005); (30): Shinozaki et al. (2006); (31): Bozzo et al. (2012); (32): Barrière et al. (2015); (33) Molina et al. (2014); (34): Maiorano et al. (2011); (35): Shu et al. (2007); (36): Iwasawa et al. (2004); (37): Landi et al. (2009); (38): Bassani et al. (2014); (39) Greenhill, Tilak & Madejski (2008); (40): Malizia et al. (2007); (41): Cardaci et al. (2011); (42): Ghisellini, Tavecchio & Ghirlanda (2009); (43): Malizia et al. (2011); (44): Edelson & Malkan (2012); (45): Landi et al. (2010b); (46):Landi et al. (2011a); (47): Tomsick et al. (2012); (48): Bassani et al. (2009); (49): Landi et al. (2010a).

This paper has been typeset from a TEX/LATEX file prepared by the author.

Downloaded from https://academic.oup.com/mnras/article-abstract/460/1/19/2608998 by guest on 29 April 2020